ISSN 1330-3651 (Print), ISSN 1848-6339 (Online) https://doi.org/10.17559/TV-20241010002049
Original scientific paper

Analysis and Testing of a Tubular Linear IPM Generator for Free Piston Engines Applied to Linear Range Extender Systems

Serdal ARSLAN, Sibel AKKAYA OY*

Abstract: This text involves the analysis and application of the tubular linear generator with interior permanent magnets design for free-piston systems using Ansys-Maxwell. A comparison of the Linear generator, whose primary part (stator) consists of 6-piece silicon steel sheet modules and its solid models including 2D and 3D models, was carried out. Although the solid models have the same motion, the effect of the decrease in packing ratio in the solid model on induced voltage, iron loss, output power, and thrust force has been examined. Additionally, by calculating the voltage constant and force constant, the percentage decreases have been determined. While the results obtained from the 2D and 3D models are quite close, a decrease of approximately 32.39% in the voltage constant and 28.06% in the force constant has been observed due to a 50.28% decrease in the packing ratio. Moreover, the reduction in approximate total mass is 38.18%, as well as the reduction in total approximate cost is 9.6%. Based on the findings from the study, a prototype of the generator has been manufactured, and an unloaded experiment has been conducted through a pneumatic setup. These experiments aim to determine how effective the design is in practical applications.

Keywords: generator; interior permanent magnets; packing factor; tubular linear

1 INTRODUCTION

These for every kilowatt-hour (kWh) of electrical energy generated in fossil fuel-based energy conversion systems, there is a release of carbon dioxide into the atmosphere. The consideration of the increase in carbon dioxide emissions per kilowatt released into the air has stimulated the quest for new energy sources and intensified efforts towards the effective and efficient utilization of existing resources. Additionally, the improvement in the efficiency of systems powered by electrical energy contributes to an overall enhancement in system efficiency, resulting not only in energy savings but also in a reduction in the formation of greenhouse gases.

In our daily lives, while circular motion systems are commonly used for linear drive systems, especially in recent years, direct-driven linear systems have become prevalent. Electric machines capable of generating electrical energy from linear motion without the need for any additional transmission or converter mechanism are referred to as linear generators. Linear generators are widely used in Archimedean wave oscillation systems, solar-powered Stirling systems, fossil fuel-powered free-piston systems in electric and/or hybrid vehicle technologies, portable linear charging systems, and vehicle suspension systems.

In the last two decades, notable studies have focused on free-piston energy conversion systems. Particularly, they are utilized as range extenders in electric propulsion systems, serving as auxiliary power units that generate electrical energy from the vehicle's consumed fuel. In this context, high-pressure and high-temperature gases produced by the combustion of fuel exert force on the piston surface, initiating the piston's movement. This force is harnessed to drive the generator. In Otto and Diesel engines, piston movement is linear and is orchestrated with a crank mechanism. By eliminating the crank mechanism, a free-piston operating system is achieved. However, for the engine to function, the generator must initially operate as a motor to create the initial movement. The free piston expander (FPE) has become a subject of research due to its advantages, including a simple structure, low friction losses, high power density, increased efficiency, reduced emission output, multiple fuel options, and the absence of additional mechanical components (such as a crank) [1-6]. Studies in this field, especially those related to linear generator/motor design and optimization, internal or external combustion engine design, and performance evaluations for different energy sources, have been prominent [7].

The working principles of AC/DC circular moving machines have been adapted to linear machines. Despite having structural differences, continuous magnet machines, especially those with permanent magnets, are preferred in free-piston expander applications when costs are disregarded, due to their high power density and efficiency [8]. In terms of magnet arrangements, radial [9-11], axial with interior permanent magnets (IPM) [12-15], and Halbach-type [16-18] models are prominent in single-sided, double-sided, and tube configurations. Sun et al. [19] have compared a single-phase tube-type IPM with a winding moving model of the same stroke length. Although the winding-moving type has low moving weight and high efficiency [20], the IPM model is considerably higher in power density [19]. Cheshmeh Beigi [21] has considered the Halbach arrangement as a design for a free-piston generator. Wang et al. [22] have optimized a Halbach-type tube linear generator with the aim of minimizing impact force and maintaining unloaded phase voltage within a specified limit using MOGA. Guo et al. [23] have performed calculations considering the lamination factor for a surface-mounted model, demonstrating that analytical, numerical, and test results are largely consistent. Arslan et al. [24] have tested the performance of a surface-mounted tube-type generator using response surface methodology and MOGA to enhance generator performance. Linear generators of the same geometric structure with surface-mounted and IPM types have been compared, showing that the IPM-type surface-mounted machine provides a higher force constant and power density compared to the IPM-type surface-mounted machine [25, 26]. Li et al. [27] have conducted FEM analysis of an IPM-type tube-type generator considering different speed profiles. The power obtained from a sinusoidal speed profile for the same rms speed value is significantly higher than that from a triangular and uniform motion profile [27]. The output power magnitude can be expressed by a second-degree equation that varies with frequency and stroke distance. Furthermore, connecting an adjustment capacitor to the linear generator and changing the impedance can increase the efficiency and output power of the generator [28-30]. Modular wide slotted design has been adapted to the IPM model [31]. When comparing slotted and slotless tube-type IPM and surface magnet motors, the slotted model offers much higher force density than slotless models [32]. The ratio of inner diameter to outer diameter, where force density is maximum, varies, and this ratio is larger in slotless models [32]. For IPM-type tubular motors, as the inner diameter/outer diameter ratio increases, the force/cost ratio decreases [12]. Souıssı et al. [33] and others have examined the effect of the tubular IPM flux-focusing tooth structure. Additionally, NdFeB material has a higher force density for both slotted and slotless models compared to Ferrite [12]. The combination of both materials affects the induced voltage in windings [34]. Zhou et al. [34] have conducted an analysis of the fault-tolerant 5-phase tubular IPM model, showing that changing the length of the last plate changes the impact force. The winding configuration has been investigated for slotted/pole-oriented IPM [35]. Additionally, due to the uneven distribution of magnetic flux density in the air gap, the force on the bearings changes. Marignetti et al. [36] have evaluated translator eccentricity for the tubular IPM. Analytical equations can be defined to achieve both an increase in force and a decrease in force ripple and magnet volume. Optimization can be performed by formulating a single objective function [37]. In their other works, Bianchi et al. [38] defined geometric dimensions parametrically for slotted and slotless models to obtain optimal geometry. A similar objective function can be defined for overall performance improvement and reduction of thrust force [8-24]. Different optimization methods can be applied, and Arslan and Akkaya Oy [39] have compared the multi-objective genetic algorithm with FEM and application results for the optimum tubular model. In these models, although magnets are present in the moving part, in flux-switching machines, the moving part is made of a single piece or modular steel material [40]. Sui et al. [41] compared single-phase single-stator and double-stator flux-switching generators with a new proposal for a single-phase flux-switching generator. Flux-switching generator designs have shown an increase in various applications. Hlaing and Myint [42] designed a tubular axial flux linear generator and tested it with a crank-slider mechanism. Aziz et al. [43], Xu et al. [44], and Ismael et al. [45] evaluated the performance of an air-operated FPE at different pressure levels.

In our previous study [13], an optimization work aiming to reduce the impact force of this model was conducted. Numerical analyses were performed in this study by considering the packing factor of the model based on the obtained dimensional magnitudes. In summary, this study evaluated the literature research, provided in the previous section, and assessed the dimensionalization and analysis results of the model discussed in the second section. The 2D and 3D models of the generator were compared with a solid shape. The primary (stator) is composed of six laminated silicon steel sheets modules forming a Segmented Core with Polygonal Cross-section (SCPC) structure, in which the windings are placed. While the solid models have the same moving part, the effect of the decrease in the packing factor in the solid model was examined on the induced voltage, iron loss, output power, and thrust force. In addition, voltage constant and force constant were calculated, and the percentage decrease amounts were determined. In the third section, the process of manufacturing a prototype of this generator and the experimental findings obtained from the pneumatic test are presented. The last section discusses the results obtained from the study.

2 TUBE TYPE IPM LINEAR GENERATOR MODEL

The in circular moving machines, torque and angular velocity are considered in power calculations, while in linear machines, power is calculated based on force and velocity [8, 13, 24]. The prototype of linear generator and its basic dimensions is shown in Fig. 1.

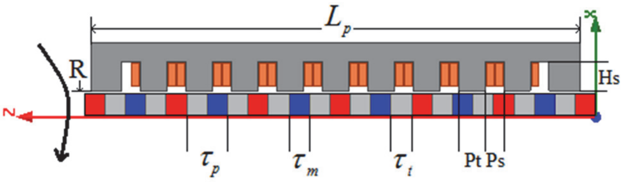

Figure 1 Half cross-sectional diagram with structural parameters of a tubular linear IPM generator (*r-z* plane)

As seen in Fig. 1, L_p is given as the primary length, and R is the expression for the radius up to the primary teeth. Synchronous velocity in permanent magnet generators is found as in Eq. (1).

$$v = 2fT_p \tag{1}$$

where, f was given as frequency and T_p was given as pole pitch. Pole pitch is the distance of *N-S* pole to the other pole.

Primer length L_p is calculated by Eq. (2).

$$L_P = T_p N_p \tag{2}$$

where, N_p is pole number.

Working distance of linear generator is expressed as stroke length (L_{str}). With its reciprocating motion, the total stroke length becomes $2L_{str}$. Consequently, the overall secondary length is determined using Eq. (3).

$$L_s = L_p + 2L_{str} \tag{3}$$

Primer teeth width (P_t) is calculated by Eq. (4).

$$P_{t=}T_{os} - P_s \tag{4}$$

where, slot width (P_s), slot pitch (T_{os}) effects electrical and magnetic charge.

Geometric sizing is given in Tab. 1.

Table 1 Design parameters of three phase, tubular linear IPM generator

Geometric	Values	Unit	Geometric	Definitions
Pole pitch (τ_p)	30	mm	Primary Steel Material	M43_24G
Tooth width (P_t)	19.75	mm	Secondary Steel Material	Steel1020
Slot width (P_s)	13.57	mm	Permanent Magnet Material	NdFe35
Primary inner diameter ($2R$)	38	mm	Winding Type	Double Layer
Height slot (H_s)	19.11	mm	Slot/Pole	9/10
Magnet width (τ_m)	15	mm	Magnet width to pole pitch ratio (α)	0.5
Air gap	2	mm	Slot width to slot pitch (β)	0.4
Rphase	2.65	ohm	Inner diameter to outer diameter ratio	0.355

Axial magnetic tube type generator has been modelled as 6 parts silicon steel sheets modules, solid and two-dimensional (Fig. 2). The module consists of an inner translator with ring-shaped permanent magnets, and the slotted primary with two layer concentrated winding. Solid model occurs when longitudinally lined laminations are packed 100%. However, in practice it is very difficult to pack sheet iron 100%. The ratio of the total lamination material to the total primary area available is 50.28% (Fig. 2. Polygonal Model or SCPC model as 6 parts silicon steel sheets modules). This ratio is thus defined as the primary lamination fill factor K_{lam} . K_{lam} is always assumed as 100% for solid model and 2D model.

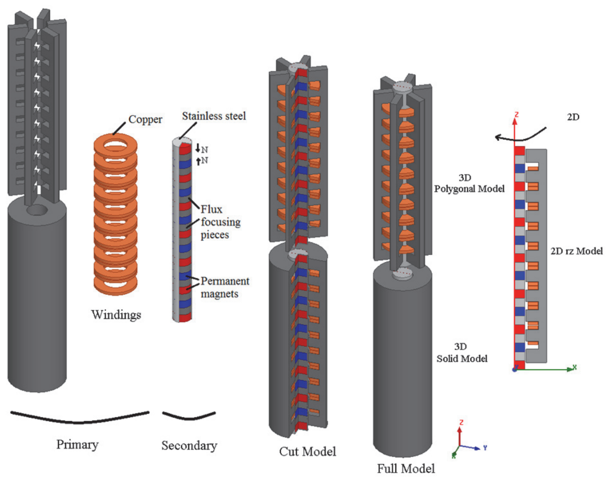

Figure 2 Illustration of tubular linear IPM generator models: 3D polygonal (above) and solid model (below)

3 ANALYSIS RESULTS AND EVALUATION

Ansys-Maxwell program was used for numerical analyses. Load analyses were conducted with three models (Fig. 3) on condition that sizing data are stator. Open-circuit simulation can be done without using an external circuit model and without connecting a load at the generator ends.

As can be seen in Fig. 4a, the induced voltage is less in Polygonal model. The primary reason for this is the decrease in magnetic flux. When the three dimensional and two dimensional solutions were examined, close results were obtained. However, two dimensional results are a bit higher than three dimensional. When outlet change under 10 ohm star connected load was examined, it was found that outlet increases as the speed increases (Fig. 4b). However, the power obtained from Polygonal model is less.

Voltage constant is known as K_v . 2D analysis result 66,66 Vs/m for the geometries given in Fig. 4a was calculated as 67.73 Vs/m in solid model and as 45.79 Vs/m in polygonal model.

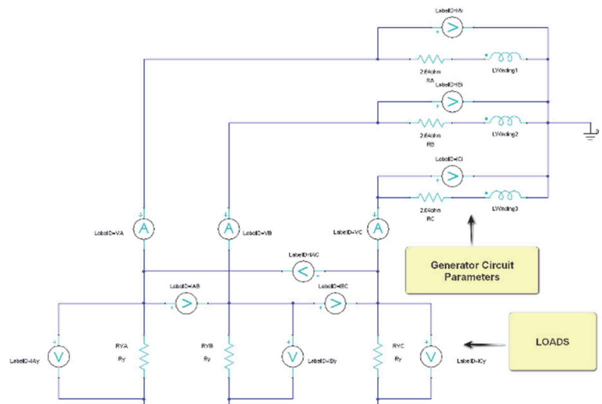

Figure 3 External circuit model of the generator for loaded simulation

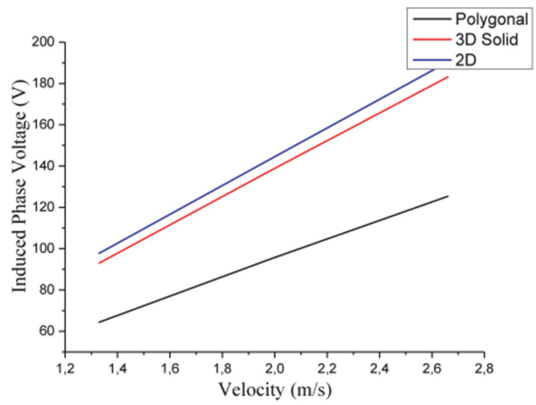

(a)

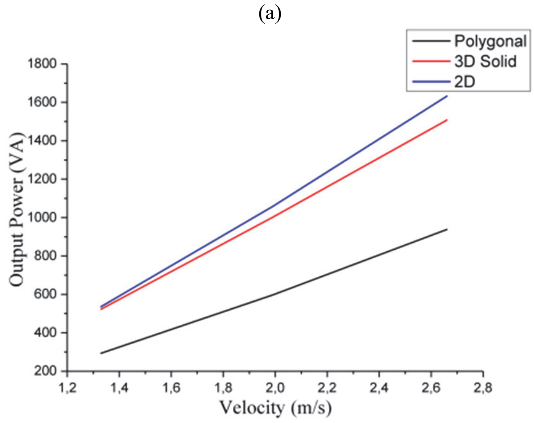

(b)

Figure 4 (a)The induced phase voltage at no-load simulation; (b) the output power and versus velocity at loaded simulation

In free piston applications, engine should operate first for the linear generator to operate. Thus, the force-current characteristic (K_f) of the machine should be known. When the current is decomposed into q and d components, the d component is set to zero for control, and the electromagnetic thrust of the machine changes proportionally with the phase current [46]. Force change according to current change in rated speed is given in Fig. 5.

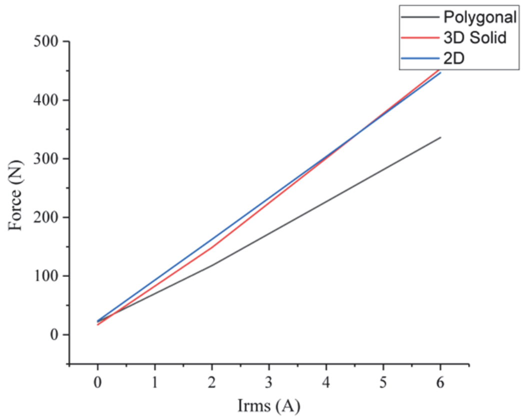

Figure 5 The force and input current for starting proccessing

Force constant is known as K_f. 2D analysis result 70.5 N/A for the geometries given in Figure 5 was calculated as 72.7 N/A in solid structure and as 52.3 N/A in polygonal structure. The reduction ratio (z, %) is defined to detect the magnitude of the difference between the solid model and the polygonal model. It is calculated as in Eq. (5).

$$z = 100\left(\frac{x-y}{x}\right) \tag{5}$$

where, x and y are the parameter values solid model and polygonal model of the linear generator.

To investigate the change in magnetic flux density due to variations in the magnet, only the magnet material was altered in a 2D solid model. In recent years, $Sm_2Fe_{17}N_3$ magnets have gained attention due to their potential to reduce the use of rare-earth elements and lower costs [47, 48]. Although their applications are still at the laboratory scale, the promising outlook for their use in electric machines, as discussed in reference [47], has led to their inclusion in this study. Some of the selected magnet materials (AlNiCo9, Y30, N35) were taken from the Ansys Maxwell V19 material library. Steel 1010 was selected as the secondary steel material in the magnetostatic analysis. The magnet materials considered in this study include Alnico 9, Ferrite Y30, Neodymium-Iron-Boron (NdFeB) grade N35, $Sm_2Fe_{17}N_3$ [47, 48], and Samarium-Cobalt grade S24 [49]. The remanent magnetization (Br) and coercive field strength (Hc) values are as follows: Alnico 9 (Br = 1.05 T, Hc = –119,366 A/m), Ferrite Y30 (Br = 0.4 T, Hc = –188,000 A/m), NdFeB N35 (Br = 1.099 T, Hc = –890,000 A/m), $Sm_2Fe_{17}N_3$ (Br = 0.972 T, Hc = –903,204 A/m) [48], and SmCo S24 (Br = 0.92 T, Hc = –661,000 A/m) [49]. The results of the 2D magnetostatic analysis are presented in Figs. 6 and 7. Fig. 6 illustrates the variation of magnetic flux density and the corresponding flux lines.

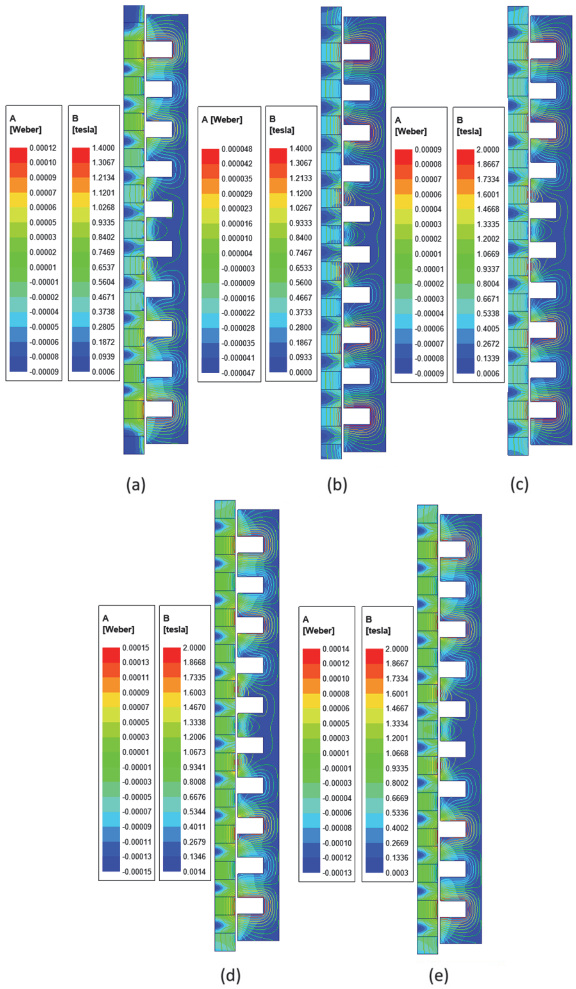

Figure 6 The magnetic flux density distribution of the tubular linear IPM generator (*r*-*z* plane); a) AlNiCo 9, b) Feritte Y30, c) SmCo S24 d) NdFeB N35 e) $Sm_2Fe_{17}N_3$

In the case of the AlNiCo material, the magnetic flux lines are fewer and more sparsely distributed. As commonly observed in material classifications, the magnetic flux density increases with the maximum energy product (BH)max. Among the tested materials, the highest magnetic flux density is observed in the N35 magnet. In Figs. 6a and 6b, demagnetization can be seen at the corner regions of the magnets. In all magnet models, the magnetic flux density decreases in the lower inner part of the secondary steel. To enhance magnetic flux concentration, the inner steel region could be removed. However, for ease of manufacturing, the secondary component was constructed using a steel ring and ring-shaped magnets. To further analyze this condition in detail, the flux density distribution within the air gap is examined in Fig. 7.

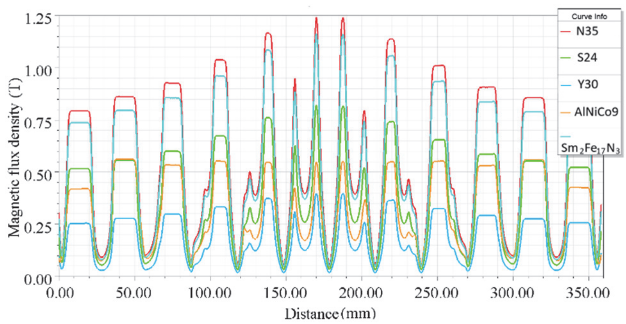

Figure 7 Variation of the air gap magnetic flux density for different magnet grades

In terms of magnetic flux density variation within the air gap, the considered magnets exhibit similar distribution patterns. However, when ranked from highest to lowest magnetic flux density, the order is as follows: N35, $Sm_2Fe_{17}N_3$, S24, AlNiCo9, and Y30. The maximum magnetic flux density achieved with the N35 magnet is approximately 1.24 T, while for the $Sm_2Fe_{17}N_3$ magnet, it is observed to be around 1.15 T. If $Sm_2Fe_{17}N_3$ magnets reach technological maturity and become commercially producible and widely available, they have the potential to compete with NdFeB magnets.

The unit cost values taken are 2.12 USD/kg for steel material, 14.85 USD/kg for copper material, and 84.87 USD/kg for magnet material (NdFeB) respectively [50]. The cost calculation is presented in Tab. 2. It does not include machine body and labor costs. Here, the primary steel density is taken as 7700 kg/m³, copper winding density as 8933 kg/m³, magnet density as 7400 kg/m³, and secondary steel density as 7700 kg/m³.

Table 2 Material costs and mass of models

Models	Primary Iron mass / kg	Cooper mass / kg	Mover mass / kg	Total mass / kg
Polygonal model	8.74	2.85	2.59	14.18
3D model	17.5	2.85	2.59	22.94

As seen in Tab. 2, the polygonal model exhibits a respective decrease of 38.8% in total mass, 9.6% in total mass, 28% in force constant, and 32.4% in voltage constant compared to the 3D solid model.

4 GENERATOR DRIVE SYSTEM THROUGH PNEUMATIC SYSTEM

The manufacturing of the tubular generator was achieved through laser cutting of sheets based on the dimensions of the designed generator. Additionally, chrome sheets were cut to fit and placed for the assembly of sheets. Since the coils are ring-shaped, molds were made from Delrin material, and the winding was done to have 75 turns. The coil resistance and phase inductance were measured using an LCR meter, resulting in a phase resistance of 2.76 ohms. The coils placed in the sheet slots are shown in Fig. 8a, and the moving part is presented in Fig. 8b. Fig. 9 shows the designed pneumatic system and application system. The experimental setup is shown in Fig. 10.

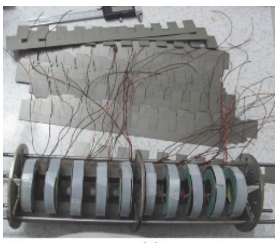

(a)

(b)

Figure 8 (a) The coils placed in the sheet slots (b) moving part

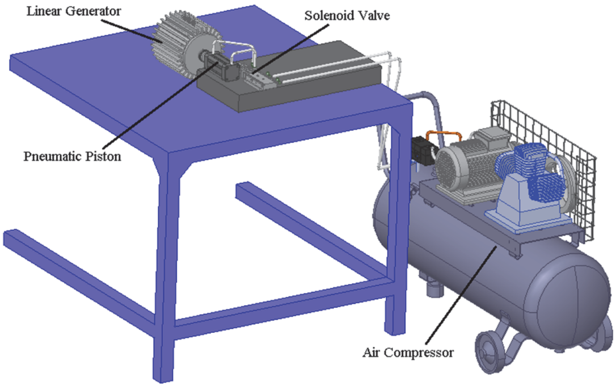

Figure 9 General scheme of pneumatic system considered for free piston energy converter using polygonal linear generator

Figure 10 Experimental module of the prototype 9/10 polygonal linear generator with pneumatic system

The changes in induced voltage due to the experimental results are presented in Fig. 11 and Fig. 12, along with the changes in induced voltage from numerical analysis.

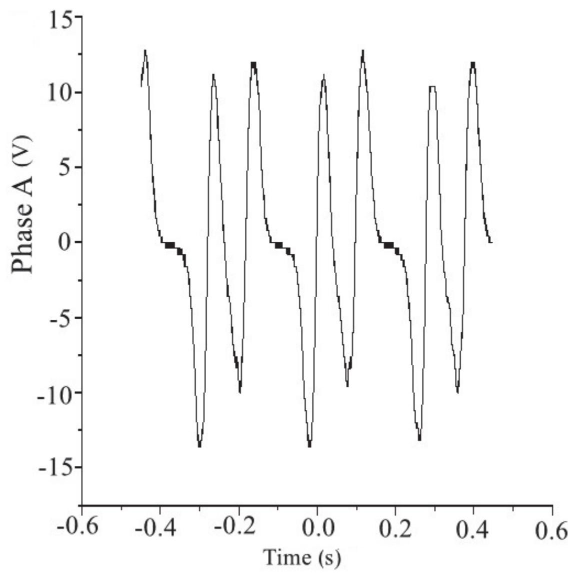

Figure 11 Phase voltage waveform from experimental results

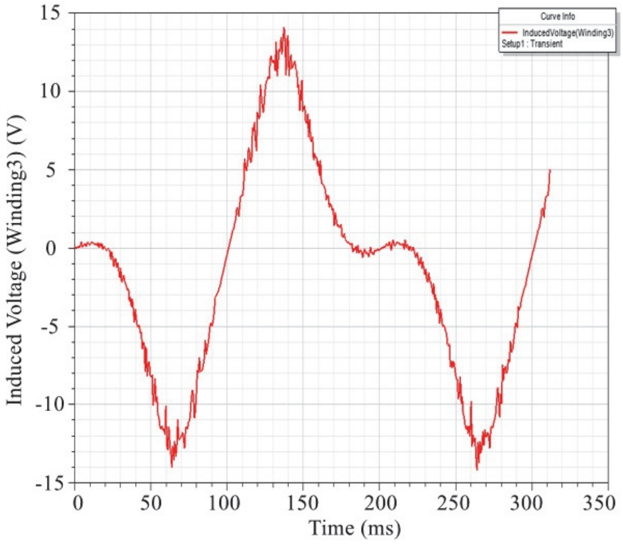

Figure 12 Phase voltage waveform from numerical analysis results

In the conducted experiment under load, the current passing through the load was observed to be 0.3 A. Due to the low speed of the pneumatic system, the induced voltage in one of the phase windings was approximately a maximum of 14 V. Although the linear generator topologies vary across different studies in the literature, the operational speed values are often kept low to avoid issues related to crank-slider or piston mechanisms and to ensure validation through simulation. A tubular model with a Halbach array configuration and a 7-pole/6-slot topology has been analyzed in [51], with the experimental study conducted at a velocity of 0.98 m/s. In [52], a double-sided model was investigated by examining the induced voltage waveforms at velocities of 0.25 m/s and 0.5 m/s. For the Free Piston Engine (FPE) generator, both experimental and simulation results were compared for a maximum velocity of 0.7 m/s [53]. In [54], design velocities of 1 m/s and 2.5 m/s were selected for the linear generator model; however, experimental measurements of the induced voltage from the generator windings were performed at lower velocities of 0.05 m/s and 0.1 m/s. In a free-piston system driven by a pneumatic mechanism, system testing was carried out at maximum velocities of 0.8 m/s under pressure conditions of 3 to 4 bar [55]. Considering these studies, it can be concluded that performing tests at lower velocities than the design speed is appropriate for evaluating both simulation and experimental results. Therefore, the generator obtained low power at low speeds in the range of 0.1-0.5 m/s. Free-piston applications operate in the speed range of 2-6 m/s. The generator is designed to deliver a maximum power of 750 W at a rated speed of 2 m/s. For mechanical reasons, in this implementation, a pneumatic system was preferred, and experiments were conducted. The pneumatic system's speed condition was analyzed using the finite element method, and the induced voltage closely matched the voltage range measured in the application.

5 CONCLUSION

As highlighted in our previous studies on free-piston systems [8, 24, 30, 39], a significant increase in such applications is expected due to advantages such as fuel flexibility, cost-effectiveness, and high efficiency. Linear generator platforms developed by Libertine FPE Ltd can deliver output power in the range of 10-30 kW and, thanks to their modular architecture, can be easily adapted to various fuel types, including LPG, biogas, and hydrogen [56]. The linear generator system developed by Mainspring Energy offers modular configurations with output power up to 240 kW [57]. The hydrogen-powered engine platform by Aquarius Engines weighs only 10 kg and has been effectively utilized in portable power systems and micro-cogeneration units [58]. The present study has been conducted with a focus on low-power applications.

This study examines the structure of a Segmented Core with Polygonal Cross-section (SCPC) linear generator for free piston applications. This structure consists of ring shaped embedded magnetic structure in longitudinal structure. Although it is like tube type geometry, it gives important advantages in terms of manufacturability and heat (providing cooling surface). In addition, the force obtained for initial starting was found to be sufficient. Although there is still a very limited number of studies on the design and application of new magnet materials in electric machines, the novel magnet type $Sm_2Fe_{17}N_3$ has also been investigated in this study. A comparative analysis of the air-gap magnetic flux density was conducted using 2D magnetostatic simulations. Among the evaluated materials, N35 was selected for practical implementation due to its high magnetic flux density and commercial availability. According to the application values obtained, generator was found to be suitable for solar energy Stirling engine drive systems and free piston applications.

This study's results can be summarized as follows;

- Two- and three-dimensional analysis results were quite close.
- In the 2D magnetostatic analysis, the air-gap magnetic flux density of the $Sm_2Fe_{17}N_3$ magnet material is comparable to that of the N35 magnet. From this perspective, $Sm_2Fe_{17}N_3$ has the potential to become a competitive alternative to rare-earth-based magnets in future applications.
- The decrease in packing rate decreased the tension constant and force constant values. Although this decrease did not occur at the same rate as the packaging ratio, the output power decreased in a similar way to the packaging ratio.
- In the SCPC model, a mass reduction of approximately 38% resulted in a decrease of about 28% in the force constant and around 32% in the voltage constant.
- It is obvious that working with silicone sheets in the manufacturing of tube type models reduces the packaging rate. However, the decrease in packaging rate can be prevented with materials such as Samoloy.
- The sizing dimensions were maintained the same in the 2D, 3D, and polygonal models, despite the decrease in the cost of the polygonal model.

A polygonal structure similar to the primer can be applied to the moving part. Thus, magnet costs and Eddy losses in magnets can be reduced. However, the effect of this cost improvement on generator parameters will be examined in future studies. Furthermore, this concept involving the use of $Sm_2Fe_{17}N_3$ material will be investigated in future work.

Acknowledgements

This paper and its related research are supported under Project AR-1507 by grants from the Ordu University, Department of Scientific Research Project Development Program of Turkey. The author would like to thank Ulupars Ltd. Sti. for its financial support in the design and laboratory testing processes.

6 REFERENCES

[1] Cawthorne, W. R., Famouri, P., Chen, J., Clark, N. N., McDaniel, T. I., Atkinson, R. J., Nandkumar, S., Atkinson, C. M., & Petreanu, S. (1999). Development of a linear alternator-engine for hybrid electric vehicle applications. *IEEE Transactions on Vehicular Technology*, *48*(6), 1797-1802. https://doi.org/10.1109/25.806767

[2] Hou, X., Ji, D., Zhou, D., & Gao, H. (2023). Simulation study and performance analysis of free piston linear generator (FPLG) used for ORC system. *Energy*, *282*, 128932. https://doi.org/10.1016/j.energy.2023.128932

[3] Özden, C. M. (2005). *Homogeneous mixture internal combustion engines.* Master's thesis, Yıldız Technical University, Institute of Science, İstanbul, Turkey.

[4] Mohamed, N. N., Ariffin, A. K., & Fonna, S. (2012). Simulation of a two-stroke spark ignition free piston linear engine motion. *Jurnal Teknologi*, *44*(1), 27-40. https://doi.org/10.11113/jt.v44.3

[5] Famouri, P., Cawthorne, W. R., Clark, N., Nandkumar, S., Atkinson, C., Atkinson, R., McDaniel, T., & Petreanu, S. (1999). Design and testing of a novel linear alternator and engine system for remote electrical power generation. *Proceedings of the IEEE Power Engineering Society 1999 Winter Meeting*, *1*, 108-112.

[6] Chen, Chen, C., Zheng, P., Tong, C., Shang, J., & Liu, B. (2022). Rectangular thrust control methods of PMLSM for stroke and dead centers tracking of free-piston linear generator. *Proceedings of the 2022 25th International Conference on Electrical Machines and Systems (ICEMS)*, 1-4.

[7] Ngwaka, U., Chen, F., Qiu, S., Li, M., Zhang, C., & Wu, D. (2023). Recent progress on performance and control of linear engine generator. *International Journal of Engine Research*, *24*(7), 2866-2896. https://doi.org/10.1177/14680874221118014

[8] Arslan, S. & Gurdal, O. (2022). Polygonal tubular linear permanent magnet generator analysis and experimental test. *Scientia Iranica*, *29*(1), 168-182. https://doi.org/10.24200/sci.2019.50094.2739

[9] Arof, H., Eid, A. M., & Nor, K. M. (2004). Permanent magnet linear generator design using finite element method. *Proceedings of the International Conference on Electrical, Electronic and Computer Engineering (ICEEC'04)*, 893-896.

[10] Chen, A., Arshad, W. M., Thelin, P., & Zheng, P. (2004). Analysis and optimization of a longitudinal flux linear actuator for hybrid electric vehicle applications. *IEEE Symposium on Vehicle Power and Propulsion*, 1-6. https://doi.org/10.1109/VPPC.2004.1336369

[11] Wang, J. & Howe, D. (2005). Influence of soft magnetic materials on the design and performance of tubular permanent magnet machines. *IEEE Transactions on Magnetics*, *41*(11), 4057-4059. https://doi.org/10.1109/TMAG.2005.855152

[12] Bianchi, N., Bolognani, S., Dalla Corte, D., & Tonel, F. (2003). Tubular linear permanent magnet motors: An overall comparison. *IEEE Transactions on Industry Applications*, *39*(2), 466-475. https://doi.org/10.1109/TIA.2003.809444

[13] Arslan, S. & Akkaya Oy, S. (2017). Design and optimization of tube type interior permanent magnets generator for free piston applications. *TEM Journal*, *6*(2), 214-221. https://doi.org/10.18421/TEM62-08

[14] Rinderknecht, F. (2013). A highly efficient energy converter for a hybrid vehicle concept-focused on the linear generator of the next generation. *Proceedings of the 8th International Conference and Exhibition on Ecological Vehicles and Renewable Energies (EVER)*, 1-6. https://doi.org/10.1109/EVER.2013.6521579

[15] Lim, J., Hong, S.-K., & Jung, H.-K. (2011). Design and analysis of 5 kW class tubular type linear generator for free-piston engine. *International Journal of Applied Electromagnetics and Mechanics*, *35*(4), 231-240. https://doi.org/10.3233/JAE-2011-1334

[16] Wang, J., Wang, W., Atallah, K., & Howe, D. (2008). Comparative studies of linear permanent magnet motor topologies for active vehicle suspension. *Proceedings of the 2008 IEEE Vehicle Power and Propulsion Conference (VPPC)*, 1-6. https://doi.org/10.1109/VPPC.2008.4677550

[17] Zhu, R., Zhang, C., Chen, J., Chen, F., & Sun, P. (2018). A permanent magnet linear electric machine for the free-piston linear generator system: Design and experimental verification. *Proceedings of the 2018 21st International Conference on Electrical Machines and Systems (ICEMS)*, 1815-1820. https://doi.org/10.23919/ICEMS.2018.8549287

[18] Sato, M., Irie, S., Zheng, J., Mizuno, T., Nishimura, F., & Naganuma, K. (2021). Generator design considering mover action to improve energy conversion efficiency in a free-piston engine generator. *Electronics*, *10*(17), 2142. https://doi.org/10.3390/electronics10172142

[19] Sun, Y., Xu, Z., Zhang, Q., Lu, J., & Liu, L. (2021). A tubular single-phase linear generator with an axially magnetized PM mover for free piston engines. *IEEJ Transactions on Electrical and Electronic Engineering*, *16*(1), 139-146. https://doi.org/10.1002/tee.23276

[20] Yang, L., Xu, Z., Liu, L., Liu, N., & Yu, H. (2019). A tubular PM linear generator with a coreless moving-coil for free-piston engines. *IEEE Transactions on Energy Conversion*, *34*(3), 1309-1316. https://doi.org/10.1109/TEC.2019.2893069

[21] Moradi Cheshmeh Beigi, H. (2020). Slot less tubular PM generator with dual quasi-Halbach magnetized PM array: Analytical and numerical magnetic field analysis. *International Journal of Numerical Modelling: Electronic Networks, Devices and Fields*, *33*(2), e2569. https://doi.org/10.1002/jnm.2569

[22] Wang, J., Xiao, J., Cheng, Y., & Huang, Z. (2022). Design and modeling of a free-piston engine generator. *Frontiers in Energy*, *17*(6), 811-821. https://doi.org/10.1007/s11708-022-0848-2

[23] Guo, R., Zhang, F., & Guo, B. (2022). Modeling and research on a laminated tubular linear oscillating generator for free-piston Stirling energy conversion. *IEEE Transactions on Magnetics*, *58*(9), Article 8205305. https://doi.org/10.1109/tmag.2022.3168894

[24] Arslan, S., Gurdal, O., & Akkaya Oy, S. (2020). Design and optimization of tubular linear permanent-magnet generator with performance improvement using response surface methodology and multi-objective genetic algorithm. *Scientia Iranica*, *27*(6), 3053-3065. https://doi.org/10.24200/sci.2018.50093.1506

[25] Sato, M., Nirei, M., Yamanaka, Y., Bu, Y., & Mizuno, T. (2021). High power density by combining of a double stator and an opposite-magnets linear generator in a dual-type free-piston engine generator. *Journal of Applied Electrochemistry*, *51*(4), 473-483. https://doi.org/10.3233/JAE-190158

[26] Jalal, A. S., Baker, N. J., & Wu, D. (2016). Design of tubular moving magnet linear alternator for use with an external combustion-free piston engine. *8th IET International*

Conference on Power Electronics, Machines and Drives (PEMD 2016), 1-6. https://doi.org/10.1049/cp.2016.0273

[27] Li, J., Zuo, Z., Liu, W., Jia, B., Feng, H., Wang, W., & Roskilly, A. P. (2023). Generating performance of a tubular permanent magnet linear generator for application on free-piston engine generator prototype with wide-ranging operating parameters. *Energy*, *278*, 127851. https://doi.org/10.1016/j.energy.2023.127851

[28] Kyuseok, L., Sungho, L. & et al. (2018). Design and experimental analysis of a 3 kW single-phase linear permanent magnet generator for Stirling engines. *IEEE Transactions on Magnetics*, *54*(11), 1-5. https://doi.org/10.1109/TMAG.2018.2847459

[29] Xiao, W., Zhang, C., Chen, F., Pei, T., & Zhao, X. (2022). Structural parameter optimization for free dual-piston linear generator based on impedance matching. *25th International Conference on Electrical Machines and Systems (ICEMS 2022)*, 1-6. https://doi.org/10.1109/ICEMS53765.2022.9983268

[30] Arslan, S. & Mellah, H. (2023). Analysis and testing of internal combustion engine driven linear alternator. *Electrical Engineering & Electromechanics*, *2023*(1), 3-9. https://doi.org/10.20998/2074-272X.2023.1.01

[31] Tan, Q., Huang, X., Li, L., & Wang, M. (2019). Analysis of flux linkage and detent force for a modular tubular permanent magnet synchronous linear motor with large slots. *IEEE Transactions on Energy Conversion*, *34*(3), 1532-1541. https://doi.org/10.1109/TEC.2019.2909399

[32] Bianchi, N., Bolognani, S., & Tonel, F. (2001). Design criteria of a tubular linear IPM motor. In *IEEE International Electric Machines and Drives Conference (IEMDC 2001)*, 1-7. https://doi.org/10.1109/IEMDC.2001.939264

[33] Souissi Souissi, A., Abdennadher, I., & Masmoudi, A. (2022). Investigation of the Effects of the Pole Shoe Geometry on the IPM T-LSM Features: Application to Free Piston Engines. *IEEE Access*, 10, 17748-17759. https://doi.org/10.1109/ACCESS.2022.3187750

[34] Zhou, H., Lu, Z., Zhao, W., Liu, G., & Xu, L. (2016). Design and analysis of low-cost tubular fault-tolerant interior permanent-magnet motor. *IEEE Transactions on Magnetics,* 52(7), 1-4. https://doi.org/10.1109/TMAG.2016.2522822

[35] Wang, J. (2015). Performance evaluation of fractional-slot tubular permanent magnet machines with low space harmonics. *Archives of Electrical Engineering*, *64*(4), 655-668. https://doi.org/10.1515/aee-2015-0039

[36] Scarano, M., Cancelliere, P., & Marignetti, F. (2006). Analytical formulation of the no-load magnetic field in IPM tubular machines with translator eccentricity. *Proceedings of the 32nd Annual Conference on IEEE Industrial Electronics (IECON 2006)*, 829-835. https://doi.org/10.1109/IECON.2006.347397

[37] Akhondi, H. & Milimonfared, J. (2009). Design and optimization of tubular permanent magnet linear motor for electric power steering system. *Journal of Asian Electric Vehicles*, *7*(2), 1283-1289. https://doi.org/10.4130/jaev.7.1283

[38] Bianchi, N., Canova, A., Gruosso, G., Repetto, M., & Tonel, F. (2001). Analytical and finite element design optimisation of a tubular linear IPM motor. COMPEL - The International *Journal for Computation and Mathematics in Electrical and Electronic Engineering*, *20*(3), 777-795. https://doi.org/10.1108/03321640110393789

[39] Arslan, S. & Akkaya Oy, S. (2023). Linear generator design for concentrating solar power technologies: Optimization and prototype development. *IET Renewable Power Generation*, *17*(15), 3712-3723. https://doi.org/10.1049/rpg2.12881

[40] Wang, J., Wang, W., Atallah, K., & Howe, D. (2008). Design considerations for tubular flux-switching permanent magnet machines. *IEEE Transactions on Magnetics*, *44*(11), 4026-4032. https://doi.org/10.1109/TMAG.2008.2002773

[41] Sui, Y., Zheng, P., Liu, Y., Wang, M., & Yin, Z. (2019). Tubular unified magnetic-field flux-switching PMLM for free-piston energy converter. *IET Electric Power Applications*, *13*(5), 625-634. https://doi.org/10.1049/iet-epa.2018.5217

[42] Hlaing, C. S. S. & Myint, Z. H. (2014). Design and analysis of tubular type linear generator for free piston engine. *International Journal of Scientific Engineering and Technology Research*, *3*(8), 1326-1330.

[43] Aziz, A. R. A., Ismael, M. A., Mohammed, S. E., Baharom, M. B., & Anwarudin, A. R. T. (2022). Effect of generator configuration on the free-piston motion and power generation of air-driven expander system. *Alexandria Engineering Journal*, *61*(4), 3093-3104. https://doi.org/10.1016/j.aej.2022.01.019

[44] Xu, Y., Xue, X., Wang, Y., & Ai, M. (2019). Performance characteristics of compressed air-driven free-piston linear generator (FPLG) system: A simulation study. *Applied Thermal Engineering*, *160*, 114013. https://doi.org/10.1016/j.applthermaleng.2019.114013

[45] Ismael, M. A., Aziz, A. R. A., Mohammed, S. E., Ayandotun, W. B., Baharom, M. B., Sallehudin, M. S., & Masri, M. M. (2021). Investigation on free-piston motion and power generation of a dual-piston air-driven expander linear generator. *Energy Reports*, *7*, 2388-2397. https://doi.org/10.1016/j.egyr.2021.06.016

[46] Zhou, Z., Fang, H., He, H., Ji, B., Zhang, Z. & et al. (2023). Demonstration of a single/dual cylinder free-piston engine generator prototype: Milestone achieved on system stability. *Energy*, *278*, 127948. https://doi.org/10.1016/j.energy.2023.127948

[47] Çirozlar, İ., Murakami, S., Nakamura, K., Ogawa, T., Yamamoto, S., Kobayashi, N., & Yamamoto, H. (2025). Characteristics of PMSM with Sm2Fe17N3/Fe16N2 Hybrid Bonded Magnets. *Journal of the Magnetics Society of Japan*, 2503R001. https://doi.org/10.3379/msjmag.2503R001

[48] HSMAG. (2025, May 10). *SmFeN rare earth permanent magnetic materials*. https://www.hsmagnets.com/blog/smfen-rare-earth-permanent-magnetic-materials/

[49] Goudsmit Samarium Cobalt Grade System. *Samarium cobalt grade system*. www.goudsmitmagnets.com

[50] Du, G. & et al. (2023). Comprehensive comparative study on permanent-magnet-assisted synchronous reluctance motors and other types of motor. *Applied Sciences*, *13*(14), 8557. https://doi.org/10.3390/app13148557

[51] Zheng, P., Tong, C., Zhao, J., Yu, B., Li, L., Bai, J., & Zhang, L. (2012). Investigation of a 7-pole/6-slot Halbach-magnetized permanent-magnet linear alternator used for free-piston stirling engines. *Journal of Applied Physics*, *111*(7). https://doi.org/10.1063/1.3672084

[52] Thi, N. H., Van Trang, N., Cong, H. T., Huy, D. H., Van Loc, H., Hiep, T. H., & Toan, V. B. (2021, August). An Investigation on Power Generation Characteristics of Linear Generator Driven by a Free-piston Engine. *2021 International Conference on System Science and Engineering (ICSSE)*, 495-499. https://doi.org/10.1109/ICSSE52844.2021.9502534

[53] Xu, Y., Zhao, D., Wang, Y., & Ai, M. (2019). Electromagnetic characteristics of permanent magnet linear generator (PMLG) applied to free-piston engine (FPE). *IEEE Access*, *7*, 48013-48023. https://doi.org/10.1109/ACCESS.2019.2909278

[54] Bao, G., Lü, Y., Wei, H., Wang, Z., & Gao, X. (2021). Research on magnetic field modulation composite linear motor in a dish-type Stirling thermoelectric generator. *Proceedings of the Chinese Society for Electrical Engineering*, *41*(22), 7821-7829. https://doi.org/10.13334/j.0258-8013.pcsee.2021.22.013

[55] Peng, B., Tong, L., Guo, C., & Huo, W. (2021). Experimental research and performance analysis of a free piston expander-linear generator coupled with a driving motor. *Energy Reports*, *7*, 1349-1359. https://doi.org/10.1016/j.egyr.2021.02.066
[56] Libertine FPE Ltd. *Linear Power Systems for Clean Distributed Energy*. https://www.libertine.co.uk
[57] Mainspring Energy. *Technical Specifications*. https://www.mainspringenergy.com
[58] Aquarius Engines. *Next Generation Linear Engine Platform*. https://www.aquariusengines.com

Contact information:

Dr. Serdal ARSLAN, Associate Professor
Organized Region Vocational Higher School,
Harran University, Sanliurfa, Turkey
E-mail: serdalarslan@harran.edu.tr

Dr. Sibel AKKAYA OY, Associate Professor
(Corresponding author)
Fatsa Faculty of Marine Sciences,
Ordu University, Ordu, Turkey
E-mail: sibelakkaya@odu.edu.tr